

THE COLOR-MAGNITUDE RELATION FOR METAL-POOR GLOBULAR CLUSTERS IN M87: CONFIRMATION FROM DEEP *HST/ACS* IMAGING¹

ERIC W. PENG^{2,3}, ANDRÉS JORDÁN^{4,5}, JOHN P. BLAKESLEE⁶, STEFFEN MIESKE⁷, PATRICK CÔTÉ⁶, LAURA FERRARESE⁶,
WILLIAM E. HARRIS⁸, JUAN P. MADRID⁸, AND GERHARDT R. MEURER⁹

Accepted for publication in the Astrophysical Journal

ABSTRACT

Metal-poor globular clusters (GCs) are our local link to the earliest epochs of star formation and galaxy building. Studies of extragalactic GC systems using deep, high-quality imaging have revealed a small but significant slope to the color-magnitude relation for metal-poor GCs in a number of galaxies. We present a study of the M87 GC system using deep, archival *HST/ACS* imaging with the F606W and F814W filters, in which we find a significant color-magnitude relation for the metal-poor GCs. The slope of this relation in the I vs. $V-I$ color-magnitude diagram ($\gamma_I = -0.024 \pm 0.006$) is perfectly consistent with expectations based on previously published results using data from the ACS Virgo Cluster Survey. The relation is driven by the most luminous GCs, those with $M_I \lesssim -10$, and its significance is largest when fitting metal-poor GCs brighter than $M_I = -7.8$, a luminosity which is ~ 1 mag fainter than our fitted Gaussian mean for the luminosity function (LF) of blue, metal-poor GCs (~ 0.8 mag fainter than the mean for all GCs). These results indicate that there is a mass scale at which the correlation begins, and is consistent with a scenario where self-enrichment drives a mass-metallicity relationship. We show that previously measured half-light radii of M87 GCs from best-fit PSF-convolved King models are consistent with the more accurate measurements in this study, and we also explain how the color-magnitude relation for metal-poor GCs is real and cannot be an artifact of the photometry. We fit Gaussian and evolved Schechter functions to the luminosity distribution of GCs across all colors, as well as divided into blue and red subpopulations, finding that the blue GCs have a brighter mean luminosity and a narrower distribution than the red GCs. Finally, we present a catalog of astrometry and photometry for 2250 M87 GCs.

Subject headings: galaxies: elliptical and lenticular, cD — galaxies: individual(M87) — galaxies: dwarf
— galaxies: evolution — galaxies: star clusters – globular clusters: general

1. INTRODUCTION

Globular clusters (GCs) contain the oldest stellar populations in galaxies, and are in many ways our most accessible link to the earliest, most intense phases of galaxy building. The formation of GC systems are clearly linked to the formation of the galaxies that host them. Well-established correlations show, for instance, that both the mean metallicity of the entire GC population and the mean metallicities of the well-known metallicity subpopulations are correlated with the masses of the hosts (e.g. Brodie & Huchra 1991; Larsen et al. 2001; Peng et al.

2006a). However, recent work has indicated that there may also be a link between the metallicities of *individual* metal-poor GCs and their masses (Harris et al. 2006; Strader et al. 2006; Mieske et al. 2006; Spitler et al. 2006; Forte et al. 2007; Cantiello, Blakeslee & Raimondo 2007; Lee et al. 2008; Wehner et al. 2008). This discovery, mainly in the GC systems of massive early-type galaxies, runs counter to the previously held conventional wisdom that individual GCs do not lie on a mass-metallicity relation. Because of their low masses, it is not expected that GCs would be able to self-enrich via successive generations of star formation in the way that galaxies do.

Recently, however, high-quality color-magnitude diagrams of some Galactic GCs and LMC star clusters show evidence of multiple stellar populations (e.g. Piotto et al. 2007), provoking theoretical work on how star clusters might be able to retain gas and form successive generations of stars (D’Ercole et al. 2008; Strader & Smith 2008; Bailin & Harris 2009). A mass-metallicity relation in metal-poor GCs is also interesting when viewed alongside the mass-metallicity relation for dwarf spheroidal galaxies (dSphs) in the Local Group (Kirby et al. 2008). Despite their very different structure, GCs and dSphs have similar stellar masses. The brightest metal-poor GCs also appear to overlap in parameter space with objects that have been dubbed Ultra-Compact Dwarfs (UCDs) or Dwarf-Globular Transition Objects (DGTOS) (e.g. Hasegan et al. 2005, Mieske et al. 2008). How it is that metal-poor GCs fit into the early epochs of galaxy

¹ Based on observations with the NASA/ESA *Hubble Space Telescope* obtained at the Space Telescope Science Institute, which is operated by the Association of Universities for Research in Astronomy, Inc., under NASA contract NAS 5-26555.

² Department of Astronomy, Peking University, Beijing 100871, China; peng@bac.pku.edu.cn

³ Kavli Institute for Astronomy and Astrophysics, Peking University, Beijing 100871, China

⁴ Departamento de Astronomía y Astrofísica, Pontificia Universidad Católica de Chile, Casilla 306, Santiago 22, Chile

⁵ Harvard-Smithsonian Center for Astrophysics, 60 Garden St., Cambridge, MA 02138

⁶ Herzberg Institute of Astrophysics, National Research Council of Canada, 5071 West Saanich Road, Victoria, BC V9E 2E7, Canada

⁷ European Southern Observatory, Alonso de Cordova 3107, Vitacura, Santiago, Chile

⁸ Department of Physics and Astronomy, McMaster University, Hamilton, ON L8S 4M1, Canada

⁹ Department of Physics and Astronomy, Johns Hopkins University, Baltimore, MD 21218

growth, and what their relation is to dwarf galaxies, is still unclear.

The question of whether or not metal-poor GCs lie on a color-magnitude (i.e. mass-metallicity relation) thus has important implications for star cluster and galaxy formation. However, because the relationship between metallicity and optical color is very steep at low metallicities, discerning this relationship requires high quality data, many GCs, and preferably a large wavelength baseline. There have been many independent detections of the metal-poor GC color-magnitude relation using a variety of data sets in a number of different galaxies (see references above), but a recent paper that analyzes deep archival *HST* imaging (Waters et al. 2009) claims not to find any significant color-magnitude relation in the Virgo cD galaxy M87 (NGC 4486), a galaxy in which two different groups have reported a detection with shallower HST data (Mieske et al. 2006; Strader et al. 2006 (hereafter S06)), and one group with ground-based data (Forte et al. 2007). Given that M87 represents possibly the best combination of proximity and GC numbers for such a study (McLaughlin 1999; Tamura et al. 2006; Peng et al. 2008), it is important to establish definitively whether or not the metal-poor GCs in M87 possess a significant relationship between color and magnitude.

In this paper, we perform an independent analysis of the same data set as used by Waters et al. (2009). Most of the techniques used for this paper were first described in the analysis of the ACS Virgo Cluster Survey (ACSVCS; Côté et al. 2004), particularly for much of the data reduction and catalog generation (Jordán et al. 2004; Jordán et al. 2005; Jordán et al. 2009), and the analysis of the color-magnitude relation of blue GCs (Mieske et al. 2006; hereafter ACSVCS XIV). We refer the reader to these papers for a more thorough description of our methods.

2. OBSERVATIONS AND DATA REDUCTION

M87 was observed for 50 orbits with the ACS Wide Field Channel (WFC) in the F606W (V_{606}) and F814W (I_{814}) filters for a microlens monitoring program (*HST* GO Program 10543, PI Baltz). In all, there were 49 usable exposures in F606W and 205 in F814W. We processed these images using the Apsis ACS IDT data pipeline (Blakeslee et al. 2003) to produce summed, geometrically corrected, cosmic ray cleaned images for each bandpass. Apsis measures the offsets and rotations of each individual exposure with respect to a master catalog that it iteratively constructs from the input images. It then uses the measured offsets and rotations to combine the images using the Drizzle software (Fruchter & Hook 2002). For this analysis, we used the Gaussian interpolation kernel and an output image scale of $0''.035 \text{ pix}^{-1}$, thus taking advantage of the very large number of dithered exposures to improve the final resolution. We initially processed the images using `pixfrac=1.0` and all results presented in this paper are from this reduction. We subsequently processed the images using `pixfrac=0.5`, and although the PSF FWHM was 10% narrower for the latter case, the differences in fitted magnitudes and sizes were completely negligible. Total exposure times for the combined images are 24500 s in F606W and 73800 s in F814W.

We assume a distance to the Virgo cluster of 16.5 Mpc (Tonry et al. 2001) with a distance modulus of $31.09 \pm$

0.03 mag from Tonry et al. (2001), corrected by the final results of the Key Project distances (Freedman et al. 2001; see discussion in Mei et al. 2005b). The SBF distance to M87 itself is consistent with the galaxy being at the center of the Virgo cluster (Blakeslee et al. 2009). At this distance, one pixel in the final image therefore corresponds to 2.80 pc.

The M87 halo light dominates the image. In order to obtain accurate photometry of the GC population, we first model and remove this light using the `ellipprof` software developed for the SBF survey of Tonry et al. (1997; see also Jordán et al. 2004). Briefly, `ellipprof` iteratively fits a series of ellipses of varying centers, ellipticities, position angles, and Fourier component perturbations to the galaxy light distribution. Once the fit has converged, it interpolates to construct a smooth model, which we subtract from the image. Figure 1 shows the central $1' \times 1'$ portion of the F814W image before and after model subtraction.

3. THE PHOTOMETRIC CATALOG

3.1. Detection and Photometry

Detection was performed with SExtractor (Bertin & Arnouts 1996) on the model subtracted images using a procedure similar to that described in Jordan et al. (2004; ACSVCS II), including the removal of large-scale model residuals with SExtractor as described there. Object detection on the final subtracted image was performed using a detection threshold of five connected pixels at a 10σ significance level. The depth of the data is such that this high threshold still allows the detection of the great majority of GCs present in the field of view, while at the same time avoiding the detection of SBF and other real, albeit much fainter features. The detections in both the F606W and F814W images were finally matched using a matching radius of $0''.1$.

Our catalog of matched sources was culled by removing objects which have a mean elongation $\epsilon \equiv a/b$, measured in the F606W and F814W filters to be $\langle \epsilon \rangle \geq 2$, as well as those with magnitudes more than 7 mag from the expected GCLF turnover. This procedure removes 47 objects, which are visibly background galaxies. We note the objects removed tend to be faint, with only two rejected objects with $I \lesssim 21$. Our catalog has 2459 GC candidates after rejecting elongated sources. The sources left at this stage are run through KINGPHOT (Jordan et al. 2005), a code that measures structural and photometric parameters by fitting the two-dimensional ACS surface brightness profiles with PSF-convolved isotropic, single-mass King (1966) models.

PSFs for the F606W and F814W bands were obtained by drizzling the position-dependent set of PSFs constructed by Anderson & King (2006). The Anderson & King (2006) PSFs are meant to be used on the geometrically distorted ACS chips, so they should be drizzled in the same fashion as the actual data in order to be used on re-sampled, drizzled frames. Reproducing the kernel and `pixfrac` used is important to determine accurate sizes. In order to measure the structural parameters, we used a fitting radius of 6 pixels ($0''.21$).

For each object classified as a globular cluster candidate, KINGPHOT is used to measure the total magnitude, King concentration index, c , and half-light radius,

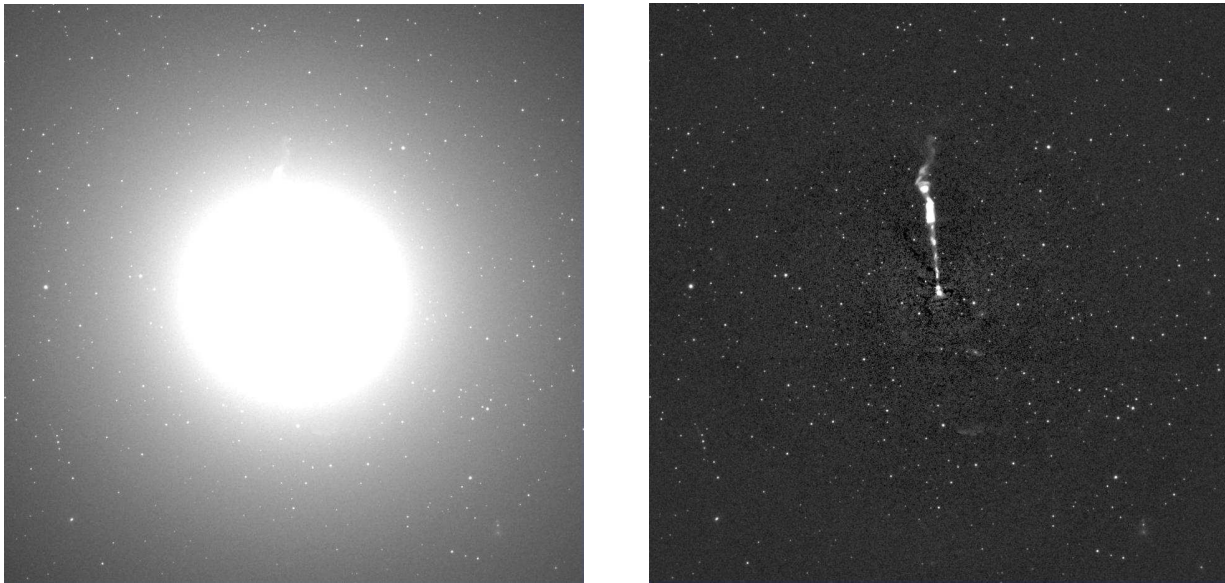


FIG. 1.— (Left) The central $1' \times 1'$ of our reduced F814W image. (Right) The same field after the subtraction of a smooth model. The point sources are nearly all globular clusters.

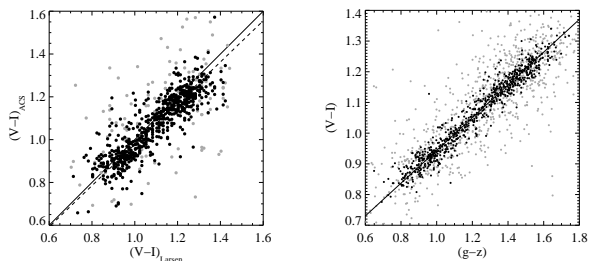


FIG. 2.— (a, left) A comparison between our $(V-I)$ photometry (y-axis) and the *WFPC2* $(V-I)$ photometry of Larsen et al. (2001, x-axis). Black points have $\sigma_{(V-I),Larsen} < 0.05$ and gray points have errors in the Larsen et al. photometry larger than 0.05 mag. The solid line has slope of unity, while the dashed line is a robust linear bisector fit to the black points. (b, right) A comparison between our $(V-I)$ photometry and the $(g-z)$ photometry from the ACSVCS. Black and gray points are those with $\sigma_{(g-z)}$ less than and greater than 0.05 mag, respectively. The line is a robust linear bisector fit to the black points.

r_h in both bandpasses. Note that these magnitudes already include the effect of size. As described in Jordan et al. (2009; ACSVCS Catalogs Paper), the magnitudes still require an aperture correction due to the fact that the PSFs used to fit the data do not extend far enough to include all of the light. We used a method identical to the one described in Jordan et al. (2009) to obtain aperture corrections using mean PSFs constructed up to a radius of $3''$ and used in Sirianni et al (2005) to derive aperture corrections. Because the magnitudes derived by KINGPHOT already include the effects of the different size of each source, the aperture corrections (A) are roughly constant with r_h , and have values of $A_{F606W} \approx 0.07$ mag and $A_{F814} \approx 0.06$ mag (we use the measured r_h for each object, averaged on both bands, to apply the aperture correction that applies to that size). Magnitudes were de-reddened using a value of $E(B-V) = 0.023$ obtained from the DIRBE maps of Schlegel et al (1998) and extinction ratios appropriate for a G2 star as presented in Sirianni et al (2005).

To produce our final sample of GCs, we rejected all

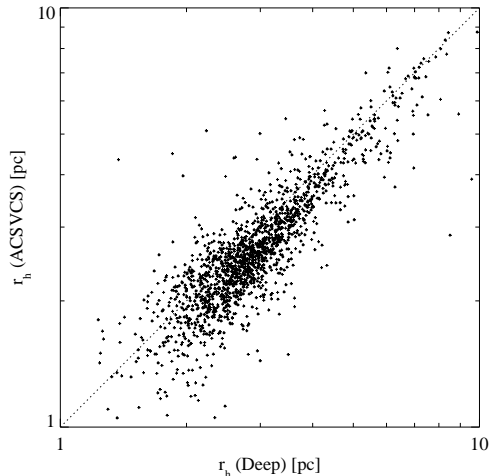


FIG. 3.— A comparison between half-light radii (r_h) measured in the single-orbit ACSVCS data and r_h measured in the deep F606W and F814W ACS images used in this study. Measurements of the same objects in these two independent data sets agree very well within the expected errors, showing that the ACSVCS data provides the necessary depth and resolution to measure GC sizes at Virgo distance. The dotted line represents a slope of unity. The slight offset from unity of 0.26 pc, which equals 3 milliarcseconds or less than one tenth of a pixel, is within the expected error from PSF systematics.

objects with magnitude errors greater than 0.5 mag in either band (116 objects), or with measured half-light radii larger than 10 pc (140 objects). Nearly all bona fide GCs, which have a mean half-light radius of 2.7 pc (Jordán et al. 2005), will qualify under this size criterion.

In order to make sure, however, that this cut does not affect our results, we used KINGPHOT to specially fit a subset of the extended objects. Because of our initial choice of fitting radius, sources with $r_h > 10$ pc have unreliable measurements (see Jordán et al. 2005 for a description of the biases that may arise when the fitting radius is less than ~ 2 times r_h). We selected the 24 extended objects with $I < 22$ mag and

TABLE 1
POSITIONS AND KINGPHOT PHOTOMETRY FOR M87 GCs

ID	RA(J2000)	Dec(J2000)	V	σ_V (mag)	I	σ_I
1	187.7432637	12.4052854	25.793	0.034	24.574	0.051
2	187.7371764	12.3819827	23.703	0.012	22.696	0.018
3	187.7341900	12.3709317	23.293	0.008	22.342	0.014
4	187.7331924	12.3676597	22.327	0.019	21.255	0.022
5	187.7340066	12.3707719	23.047	0.009	21.927	0.014

NOTE. — The complete version of this table is in the electronic edition of the Journal.

$0.7 < (V - I) < 1.5$ mag for re-fitting with KINGPHOT using a fitting radius of 18 pixels (50 pc). Of these 24 objects, 5 have very large sizes and are clearly background galaxies, and one was identified spectroscopically as a background galaxy by Hasegan et al. (2005). Of the remaining 18, the five most luminous, extended objects are in fact ultra-compact dwarfs (UCDs) or dwarf-globular transition objects (DGTOs) identified by Hasegan et al. (2005). Whether or not they should be included in a sample of GCs is debatable, but including or excluding them does not affect the results of this study. The 116 remaining fainter extended objects (likely background galaxies) are not in an important magnitude or color range for this study, and were excluded from our analysis. Our final GC catalog contains 2250 sources.

Instrumental magnitudes were converted to VEGA-MAG magnitudes in the F606W and F814W filters using zeropoints of 26.398 and 25.501 mag, respectively (Sirianni et al. 2005). Conversion of these magnitudes to V and I is not altogether advisable, as this conversion depends on the spectrum of the sources, but is necessary for comparison purposes. We converted magnitudes to V and I by using the relation between $(V - I)$ and $(m_{F606W} - m_{F814W})$ presented in Equation (3) of DeGraaff et al (2007), namely $(V - I) = 1.2(m_{F606W} - m_{F814W}) + 0.06$, and the following equation from Table 22 in Sirianni et al., $I = m_{F814W,OBMAG} + 25.495 - 0.002(V - I)$ (see discussion in DeGraaff et al. as to why our adopted color transformation is preferred to either the observed or synthetic transformations presented in Sirianni et al; the relation between I and m_{F814W} is less problematic, with the observed and synthetic transformations presented in Sirianni et al. being almost identical).

The full table of 2250 GC positions and KINGPHOT V and I photometry is presented in Table 1. We set the zeropoint of the astrometry to the International Celestial Reference Frame (ICRF; Fey et al. 2004). We did this by first matching 1579 matched GCs with the ACSVCS catalog and determining the median offsets between the two catalogs in RA and Dec, both of which were less than $1''$. The dispersion about the median offset between the two catalogs was very small ($\sigma = 0.012''$). We then calibrate the astrometry directly to the ICRF by measuring the position of the nucleus of M87 in the ACSVCS F475W image, and compare it to the position measured by Fey et al. (2004) using very long baseline interferometry radio observations.

3.2. Photometric and Size Comparisons

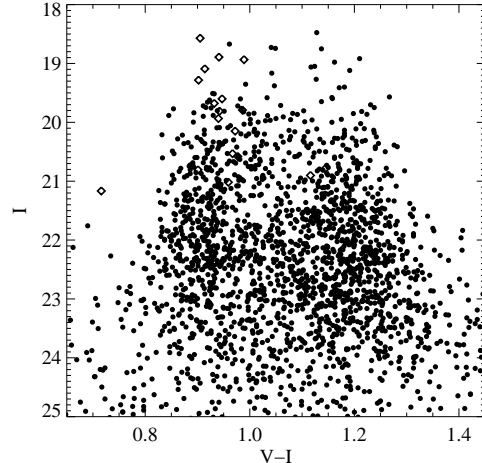


FIG. 4.— The $V-I$ color-magnitude diagram of 2250 M87 globular clusters (dots). Overplotted as diamonds are 18 objects with $r_h > 10$ pc, some of which are confirmed UCDs or DGTOs (Hasegan et al. 2005). Excluding these more extended objects from our analysis has a no impact on our results.

Because the quality of the photometry is one of the core issues for this analysis, we present comparisons between this photometry and those from two previous studies. First, we compare to the V and I photometry from the deep *HST/WFPC2* study of Larsen et al. (2001). This study used the F555W and F814W filters and transformed to V and I . We matched 757 objects between the two catalogs that were within a radius of $0''.2$. The WFPC2 field of view is smaller than that of ACS/WFC, and contains fewer objects overall. Figure 2a shows the comparison between the two photometric catalogs. We fit the objects with low error ($\sigma_{(V-I)Larsen} < 0.05$ mag) with a robust linear bisector to obtain $(V - I)_{ACS} = 0.015 + 0.963(V - I)_{Larsen}$, a relation that very nearly has a slope of unity, showing that our photometry is consistent with that from the Larsen et al. (2001) study.

Next, we compare to the ACS F475W and F850LP (hereafter g and z) photometry from the ACSVCS. Figure 2b shows this comparison using a matched catalog between the two data sets created with a matching radius of $0''.1$. The $(V-I)$ and $(g-z)$ colors are well-correlated, and a robust linear bisector fit to the high signal-to-noise data ($\sigma_{(g-z)} < 0.05$) produces the relation $(V - I) = 0.944 + 0.534\{(g - z) - 1\}$ (normalized to $(g - z) = 1$ for convenience). This is nearly identical to the relation fit by Peng et al. (2006b). Again, the shallower and deeper data are consistent within the internal uncertainties of both data sets.

Lastly, we compare the measured half-light radii, r_h between the ACSVCS data and the much higher signal-to-noise ACS data in this study. The ability to measure the sizes of the GCs is not only scientifically interesting in its own right, but is critical for photometry because the magnitudes are affected by the derived r_h . Figure 3 shows the comparison between r_h measured independently in the two data sets. We find that there is excellent correlation and agreement between half-light radii measured in the shallower ACSVCS data and those measured in the current deep ACS data for the same objects. There

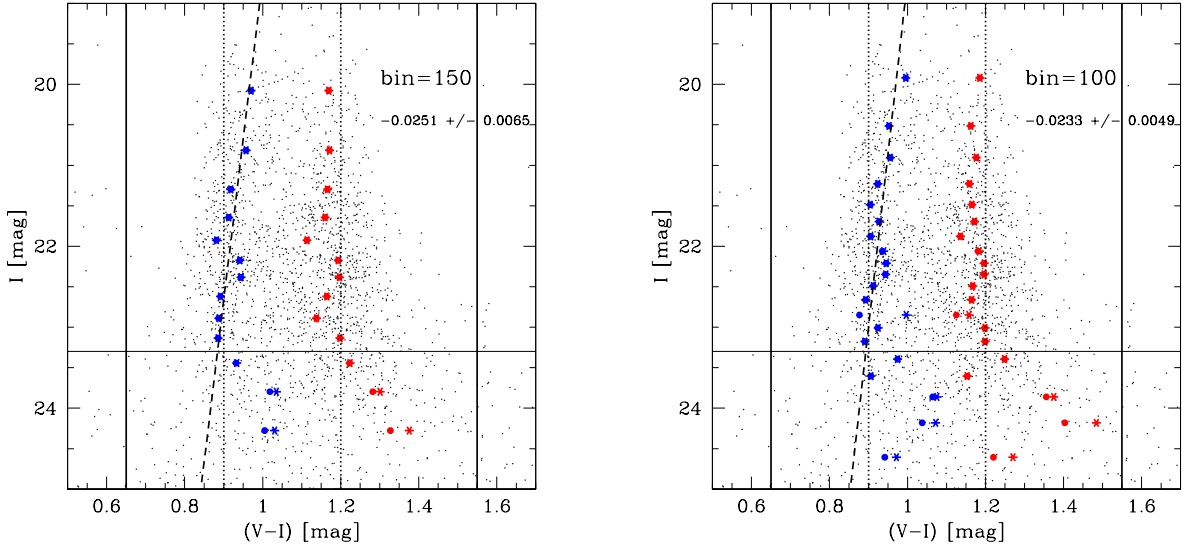


FIG. 5.— Color-magnitude diagram of M87’s GC system from the deep HST imaging set. KMM fit results are indicated, analogous to Figures 1 and 2 of ACSVCS XIV. Left panel corresponds to a luminosity bin size of $N=150$, right panel to $N=100$. We fit a linear relation to the KMM blue peak position. The dashed lines indicate fit to data points with $-12 < M_I < -7.8$ mag ($19 < I < 23.3$ mag, horizontal solid line). The two vertical solid lines indicate the blue and red color limit we adopted for fitting the KMM peak positions. The corresponding slope values are given in the plot legend, and also in Table 2.

is a slight offset of median 0.26 pc between the measured radii, which is consistent with the expected systematic uncertainty from the different PSFs used in the different filters. This offset is equal to $0''.003$ on the sky, or less than 0.1 pixels on the ACS/WFC detector. Both Kundu (2008) and Waters et al. (2009) claim that the single-orbit ACSVCS data might not be deep enough for an accurate measure of GC size, but Jordán et al. (2005) already used simulations to show that accurate sizes can be measured in the ACSVCS data, and we now confirm this empirically using the deeper data in the present study.

4. THE GC COLOR-MAGNITUDE DIAGRAM AND FITTED RELATIONS

4.1. Fitting the Color-Magnitude Relations

In Figure 4 we present the $(V-I)$ M87 globular cluster color-magnitude diagram (CMD). The two color subpopulations, blue and red, are clearly visible, with a division around $(V-I) \approx 1.05$. The typical error in $(V-I)$ for GCs with $I < 23.5$, is $\sigma_{(V-I)} < 0.02$ mag. We have also overplotted the 18 extended objects with $r_h > 10$ pc to show where they lie in the CMD. The brightest five objects with colors similar to the metal-poor GCs are UCD/DGTOs identified by Hasegan et al. (2005). The following analysis does not include the extended objects, although we have performed the analysis on the combined sample and find virtually no difference in the results.

We analyzed the luminosity dependence of the GC colors in this CMD in an identical fashion as in ACSVCS XIV. In brief, we apply the heteroscedastic mode of *KMM* to the CMD, subdivided into luminosity bins containing the same number of data points. We use two different bin sizes of $N=100$ and $N=150$ to quantify how much the result depends on the specific binning chosen. The fitted mean positions of the blue and red peaks are plotted over the respective CMDs in Figure 5, as a function of magnitude. Apart from varying the bin

size, we also choose two different pairs of initial guesses for the blue and red peak: $(V-I) = 0.9$ and 1.15 , and $(V-I) = 1.0$ and 1.25 . Finally, we adopted limiting magnitudes of $-12 < M_I < -7.8$ mag ($19.0 < I < 23.3$ mag) for the fitting. We fit linear relations to the *KMM* peak positions for all pairs of initial guesses, bin sizes and limiting magnitudes.

For each bin size, the slope $\gamma_I = \frac{d(V-I)}{dI}$ is adopted as the mean of the value derived from the two pairs of initial guesses. The errors of the fit are derived from re-sampling the points using the observed scatter around the fitted relation for the dispersion. The difference between the slopes derived from peak positions of the two different initial guesses was negligible compared to the formal fit errors. In Table 2 we give the resulting values of the slope γ_I for both the blue and red peak, for the two bin sizes, and for the average of the two. In the end, the fitted value for the slope is robust to the exact choice of bin size. For the remainder of this paper, we use the average γ_I of the fits in the two bin sizes, giving $\gamma_{I,\text{blue}} = -0.024 \pm 0.006$, and $\gamma_{I,\text{red}} = +0.003 \pm 0.007$.

To check the effect of excluding extended, UCD-like objects, we also perform the above analysis including the 18 extended sources. Doing so only changes $\gamma_{I,\text{blue}}$ by 0.001, which is much smaller than the uncertainty. We have also checked the color-magnitude diagram using the SExtractor `mag_auto` aperture photometry to make sure that the color-magnitude relation is not affected by our GC selection in general. Of the objects rejected by the size criterion, nearly all are either too faint ($I > 22.5$) or too red ($(V-I) > 1.1$) to impact our analysis of the metal-poor GCs. We have performed our analysis including all sources that make our initial SExtractor detection threshold, and find that doing so does not change our conclusions.

We emphasize that these observations are extremely deep, and that the scatter in the color-magnitude diagram is caused by physical variations in color, not

TABLE 2
 COLOR-MAGNITUDE TRENDS FOR BLUE AND RED GLOBULAR CLUSTERS BELONGING TO M87, DETERMINED WITH *KMM* FITS

Sample	$\gamma_{I,\text{blue}}$	$\gamma_{I,\text{red}}$
N=100, $M_{I,\text{faint}} = -7.8$	-0.0232 ± 0.0049	$+0.0033 \pm 0.0052$
N=150, $M_{I,\text{faint}} = -7.8$	-0.0251 ± 0.0065	$+0.0026 \pm 0.0079$
Average	-0.0241 ± 0.0057	$+0.0030 \pm 0.0066$

Notes: Columns 2 and 3 give the slopes $\gamma_I = \frac{d(V-I)}{dI}$ of the blue and red GC subpopulations, as derived from linear fits to *KMM* determined peak positions (see text and caption of Figure 5). Errors are from random resampling of the data points using their measured dispersion around the fit.

photometric error. Therefore, the uncertainty in the measurement of the color-magnitude relation is intrinsic to the population of GCs, and cannot be improved without more GCs.

4.2. The Slope Dependence on Limiting Magnitudes

We also investigate this dependence of the slope on limiting magnitudes in order to find the luminosity range over which the correlation is most prevalent. There have been previous suggestions that the slope in the blue GCs is more strongly defined by the more luminous GCs (Harris et al. 2006; Harris 2009). We quantify this more directly by performing our analysis using a range of faint and bright limiting magnitudes.

In Figure 6, we fit the blue GCs in the same way as described above, but varying the faint magnitude cut within the range $-8.7 < M_I < -7.5$, in steps of 0.1 mag. These fits show that the slope is consistently at the same value when fitting only the brightest GCs and is at maximum significance when the blue GC faint limit is $M_I < -7.8$. This corresponds to a luminosity 1.1 mag fainter than the Gaussian mean of the GC luminosity function for blue, metal-poor GCs, and 0.8 mag fainter than the GCLF turnover for all GCs (see Appendix A).

In Figure 7, we fit the blue GCs in the same way as described above, but varying the *bright* magnitude cut within the range $-12.1 < M_I < -9.0$, in steps of 0.2 mag. In this figure, the fitted slope rapidly declines as the most luminous GCs are excluded from the fit. It is clear that slope is driven by the bright blue GCs with $M_I \lesssim -10$.

However the sample is fitted, we cannot avoid the conclusion that the metal-poor GCs in the bright half of the GCLF possess a significant color-magnitude relation. This relation is driven by the most luminous blue GCs, but continues to rise in significance with the inclusion of GCs down to $M_I = -7.8$, about 1 mag below the Gaussian mean of the blue GCLF. The metal-rich GCs possess no significant slope.

5. DISCUSSION

5.1. Comparisons to Previous Estimates

There have now been many estimates of the slope of the metal-poor GC color-magnitude relation, but they have often been done in different filter systems with different instruments. More importantly, these slopes are

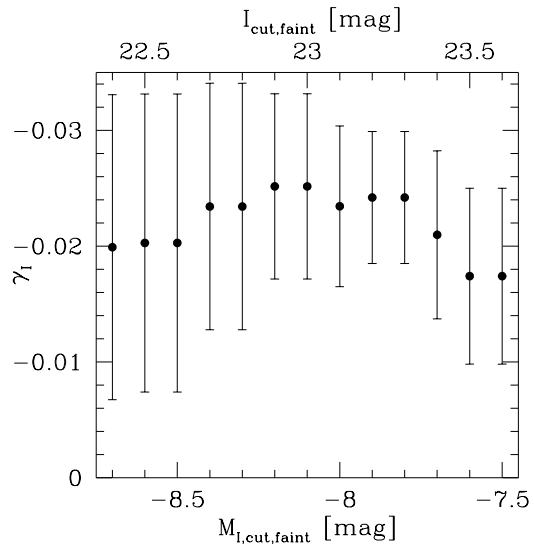


FIG. 6.— We show the fitted slope (γ_I) as a function of the faint end limiting magnitude of the metal-poor GCS used in the fit ($M_{I,\text{cut},\text{faint}}$). We find that the color-magnitude relation has a similar slope for all samples down to $M_{I,\text{cut},\text{faint}} \approx -7.8$ and has maximum significance at this limit. Including GCs fainter than this limit, or approximately 0.5 mag fainter than the turnover of the GCLF, has the effect of beginning to wash the trend out.

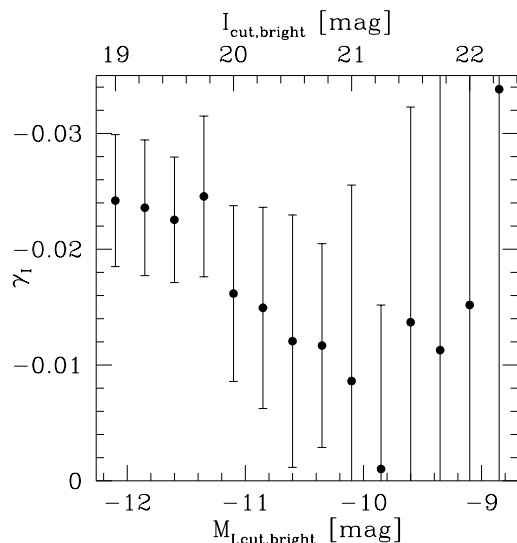


FIG. 7.— We show the fitted slope (γ_I) as a function of the bright end limiting magnitude of the metal-poor GCS used in the fit ($M_{I,\text{cut},\text{bright}}$). We find that the color-magnitude relation is driven by the most luminous GCs, or those with $M_I \lesssim -10$. For this plot, we assumed $M_{I,\text{cut},\text{faint}} = -7.8$.

usually transformed into a mass-metallicity relation using a metallicity-color relation derived from either Galactic GCs or stellar population synthesis models. Although transforming to physical quantities is important for understanding the ultimate origin of this phenomenon, we stress that for comparisons between different studies it is the slopes in *observed quantities* (color and magnitude) that should be compared rather than in the transformed quantities (metallicity and mass). This is for the simple reason that transformations between different filter sets and colors are much more precisely known than the transformation from color to metallicity. Direct compar-

isons in mass-metallicity space that do not take this into account can produce misleading results, as we will describe below for the case of Waters et al. (2009).

The fits in ACSVCS XIV used a limiting magnitude of $M_z = -7.7$, which closely matches a magnitude limit of $M_I = -7.8$ (the g_z photometry is on the AB system while VI is VEGAMAG). Thus, for the purposes of our comparison, we will use the average of the measured slope values fitted to samples with a limiting magnitude of $M_I = -7.8$, which is $\gamma_I = -0.022$. In ACSVCS XIV, the measured slope for M87's metal-poor GCs is $\gamma_z = \frac{d(g-z)}{dz} = -0.042 \pm 0.015$. This is virtually identical to that measured by S06, $\gamma_z = -0.043 \pm 0.010$. Assuming that the slope measured in ACSVCS XIV is correct, what would be the expected slope in the V and I bandpasses used for this study? We have already above in Section 3.2 matched 1637 objects in common between our current catalog and the ACSVCS catalog for M87. The fit between $V-I$ and $g-z$ presented above for these objects yields a slope of 0.534. Likewise, $I = z - 0.342 + 0.225(g-z)$. Therefore, to transform from γ_z to γ_I we use the relation:

$$\gamma_I = \gamma_z \frac{d(V-I)}{d(g-z)} \frac{dz}{dI} = \gamma_z \times \frac{0.534}{1 + 0.225\gamma_z} \quad (1)$$

For $\gamma_z = -0.042 \pm 0.015$ from ACSVCS XIV, we therefore expect $\gamma_I = -0.022 \pm 0.008$. This value is indistinguishable from the slope we derived in the previous section, $\gamma_I = -0.024 \pm 0.006$, and thus the color-magnitude relation for the original, single-orbit, ACSVCS g and z imaging is perfectly consistent with that derived from the deep, 50-orbit V_{606} and I_{814} observations analyzed here.

5.2. $m_{606} - m_{814}$ versus $g - z$: Depth, Wavelength Baseline, and the Color-Magnitude Relation

The advantage of the ACS data analyzed in this paper and in Waters et al. (2009) is the unparalleled depth compared to other imaging of M87. However, for the purpose of detecting a mass-metallicity relation in the metal-poor GCs, this data has the singular disadvantage of a short wavelength baseline. Because the filters are F606W and F814W, the baseline is shorter than even the traditional V and I to which the instrumental colors are transformed. Given the transformations used in this paper ($m_{606} - m_{814}$) \propto $0.445(g-z)$. Thus, the errors in ($m_{606} - m_{814}$) need to be 0.445 times smaller than in ($g-z$) to achieve the same metallicity sensitivity, corresponding to a higher S/N by a factor of 2.25. In the case of the observations used here, the median ratio between the error in ($m_{606} - m_{814}$) and the ACSVCS error in ($g-z$) for objects in common is 0.229. These observations are thus in principle between 1.7 and 2 times more sensitive to metallicity than the ACSVCS observations until scatter in the color become dominated by systematic error at the bright end, or by the intrinsic scatter in color among GCs (the latter is the case for our observations). Although the ratio of *HST* orbits is 50:1, the short wavelength baseline of the filters used and the intrinsic scatter of color among GCs explains why these observations are not nearly as much of an improvement over the ACSVCS as one might initially expect.

5.3. The Discrepancy with Waters et al. (2009)

The main conclusion of Waters et al. (2009) was that they did not detect a color-magnitude relation for the metal-poor GCs in M87 using deeper imaging than had previously been analyzed. In this paper, however, we have performed an independent analysis and reduction of the same archival data, and we find a color-magnitude relation with the exact slope expected from the results of ACSVCS XIV and S06. In this section, we make three comments on the claims, results, and methodology adopted by Waters et al. (2009).

5.3.1. The Color-Magnitude Relation of Blue GCs is not an Observational Artifact.

Both Waters et al. (2009) and Kundu (2008) make the argument that the color-magnitude relation previously detected for blue GCs is due to improperly performing standard aperture photometry of resolved GCs. The basic claim is that if metal-poor GCs have a size-luminosity relation where more luminous GCs are larger, then applying a single aperture correction to all objects leads to biases in color that correlate with magnitude. This claim is can be disproven in three ways.

First, both this study and the ACSVCS XIV study of the GC color-magnitude relation use photometry that *always explicitly take into account the size of the GC*. As explained above, and in Jordán et al. (2005, 2009), we use model magnitudes derived from PSF-convolved King model fits.

Second, Kundu (2008) and Waters et al. (2009) further claim that the ACSVCS data is not deep enough to measure the sizes of GCs at Virgo distance. As has been shown using simulations (Jordán et al. 2005) and now comparing to the deep ACS data analyzed in this paper, reliable sizes and photometry can in fact be derived from the shallower ACSVCS data used as the basis for previous detections of the blue GC color-magnitude relation. Moreover, the scatter in the size-luminosity relation for GCs is much more important than its slope, which is shallow and only relevant for the highest luminosity GCs.

Third, a simple test shows that even if one were to perform standard aperture photometry on resolved GCs of different sizes, the resulting bias in *color* is much too small to create the observed color-magnitude relation. Jordán et al. (2009) performed simple 4 pixel radius aperture photometry on PSF-convolved King models with a range of sizes. They found that although the total flux of GCs can be significantly underestimated for $r_h > 3$ pc, the color of the GC is only minimally affected. With $1 < r_h < 30$ pc, the ($g-z$) aperture correction deviates by only $^{+0.004}_{-0.014}$ from the $r_h = 3$ pc fiducial. For this kind of simple photometry, the different sizes of the PSFs in F475W and F850LP indeed cause the measured ($g-z$) color to become increasingly biased to the red up to a maximum of 0.004 mag at $r_h \sim 7$ pc. However, at larger sizes the bias *reverses direction* and the measured GC colors start becoming biased to the blue. This can be explained because for larger sizes, we enter the regime where the size difference between the PSFs in the two filters are small compared to the size of the GC (10 pc \sim $0''.125$ at Virgo). Therefore, even for simple 4-pixel aperture photometry, there is no conspiracy be-

tween size and magnitude that can artificially produce the color-magnitude relation in the blue GCs. This explains how slopes determined from different studies — those accounting for GC size (ACSVCS XIV, this paper), or simply applying an average aperture correction (S06), or with galaxies at different distances (Harris et al. 2006), or with data from the ground where GCs are unresolved (e.g. Forte et al. 2007; Wehner et al. 2008) — all find similar results. (See also a discussion on aperture corrections in Harris 2009; Harris et al. 2009).

5.3.2. *The Color-Magnitude Diagram of Waters et al. (2009) shows Significant Scatter.*

Despite the high signal-to-noise of these deep ACS F606W and F814W observations, the M87 GC color-magnitude diagram presented in Figure 2 of Waters et al. (2009) appears to contain a large amount of scatter. This is in contrast to the CMD presented in this paper which uses the same data (Figure 4), as well as the $(g-z)$ CMDs in Figure 1 of ACSVCS XIV, and in Figure 4 of S06. In particular, we draw the reader’s attention to the many bright blue sources in the Waters et al. CMD, those with $I < 22$ and $(V - I) < 0.9$, of which there are at least 46 shown. By contrast, our catalog generated from the same imaging contains only 2 objects (6 before the various cuts described in Section 3.1) in the equivalent region ($I < 22$ and $(V - I) < 0.8$, because we adopt the DeGraaff et al. (2007) transformation for V and I as opposed to the one from Sirianni et al. (2005), resulting in a ~ 0.1 mag shift at these colors). We do not know the cause for this difference, but we note that none of the recently published GC CMDs for M87, including Waters et al. (2006), show evidence for sources that are so luminous and blue. The same kind of disagreement is seen for luminous red sources, with $(V - I) > 1.3$. Given the short wavelength baseline of this filter set, any increase in the photometric scatter would make it extremely difficult to detect a color-magnitude relation in the blue GCs of $\gamma_I \approx 0.02$.

In addition, we note that Waters et al. (2009) use the flux within a 4-pixel aperture to perform their concentration-dependent aperture corrections. Thus, the amount of raw information they use to derive their photometry for each object is no different from that used by KINGPHOT except that their photometry is not from direct King model fits. Their analysis, therefore, does not include any additional flux or information as compared to ours.

5.3.3. *The Importance of Comparing Color-Magnitude Relations Instead of Mass-Metallicity Relations.*

There are many transformations between GC color and metallicity in the literature, based on different data sets. Most studies either derive an empirical relation from the known colors and metallicities of Galactic globular clusters, or they use models of simple stellar populations. What has become clear over the years is that the relationship between optical color and metallicity for old stellar populations is nonlinear, and becomes increasingly steep for metal-poor objects ($[\text{Fe}/\text{H}] \lesssim -1$) (Cohen et al. 2003, Peng et al. 2006a, Cantiello & Blakeslee 2007). This is exactly the color and metallicity regime with which we are concerned in this paper and in all studies of metal-poor GCs.

Although it is necessary and even desirable to transform color-magnitude relations into mass-metallicity relations, it is important that observational comparisons be done *directly*, rather than through the minefield of different metallicity-color relations. Waters et al. (2009) do not compare colors directly, but instead attempt to simulate slopes in their data starting with mass-metallicity relations. The $[\text{Fe}/\text{H}]-(V-I)$ relationship assumed by Waters et al. (2009), however, is inconsistent with the $[\text{Fe}/\text{H}]-(g-z)$ relations assumed in ACSVCS XIV and S06; $(V-I)$ is less sensitive than to $[\text{Fe}/\text{H}]$ than $(g-z)$, particularly at low metallicity. This leads Waters et al. to conclude that the expected slope would be much more easily seen in their data than it actually is. Furthermore, their simulated CMD takes the brighter GCs as fixed and offsets GCs with $I > 20$ to the blue. If they had instead fixed the GCs around the GCLF turnover and then offset brighter ($I < 23$) GCs to the red the expected trend would be more difficult to detect. As a result, they generate a large gap between the blue and red GC populations that, in their Figure 3a, bears no resemblance to a real CMD. If previous authors had observed such a CMD to derive a color-magnitude relation, there would be little argument about its existence. The simulations of Mieske et al. (2006), which were performed in color space alone, are better suited to testing the sensitivity of observations to any color-magnitude relation.

5.4. *Substructure in the Color-Magnitude Diagram*

Having established the existence of a color-magnitude relation for metal-poor GCs, it is still not clear what its underlying cause might be. The high photometric accuracy of this data set, however, shows some tantalizing hints at substructure in the color-magnitude diagram shown in Figure 4, especially in the blue GCs. While there is an obvious ridge of blue GCs that appears to be driving the color-magnitude relation for $21 < I < 23$, there are also clusterings of GCs in the CMD at higher luminosities and intermediate colors, as well as “void” around $(V-I) \approx 1.0$ and $I \approx 21.5$. Given the precariousness of transforming from broadband color to metallicity for stellar populations with $[\text{Fe}/\text{H}] \lesssim -1$ (e.g., Peng et al. 2006a; Yoon et al. 2006; Cantiello & Blakeslee 2007), we do not wish to over-interpret these groupings. It is possible, however, that this clustering, which appear to strengthen the observed color-magnitude relation, may be the sign of an intermediate population of GCs.

6. CONCLUSIONS

We present an analysis of the color-magnitude diagram and luminosity functions for globular clusters in the Virgo cD galaxy, M87, using deep, archival *HST/ACS* imaging in the F606W and F814W filters. We report an independent detection at high significance (4σ) of a color-magnitude relation for the blue GCs, which was previously reported for this galaxy using shallower data from the ACSVCS (Mieske et al. 2006; S06). The measured slope in $(V-I)$ is entirely consistent with the previously published values in $(g-z)$. This finding is contrary to a recent independent reduction and analysis of the same deep archival data by Waters et al. (2009) who claim to find no relation.

We fit the color-magnitude relation for a range of faint and bright limiting magnitudes, M_I , to test the idea that

the bright GCs drive the relation. We find that the slope is driven by GCs brighter than $M_I \approx -10$, and is most significant for samples including GCs brighter than $M_I = -7.8$, or 1 mag fainter than the mean of the blue GCLF, or 0.8 mag fainter than the mean of the total GCLF. This suggests that there is a mass scale at which the correlation between mass and metallicity begins, and is qualitatively consistent with a scenario where self-enrichment drives the relation (Bailin & Harris 2009).

All of our photometry is performed using the King model fitter, KINGPHOT (Jordán et al. 2005), and explicitly takes into account the size of each object. We show that the half-light radii previously measured using KINGPHOT on the shallower ACSVCS data in Jordán et al. (2005) are well-correlated with the new, more accurate measurements.

We explain that the color-magnitude relation seen in the metal-poor GCs cannot be an observational artifact involving aperture corrections, as argued by Kundu (2008) and Waters et al. (2009). All of our photometry

explicitly uses the fitted size of the object to derive total magnitudes and colors. We also show that even if one were to use a fixed aperture correction for all GCs (as in S06 and Harris et al. 2006), the magnitude of the bias is much too small to create the observed color-magnitude relations.

We thank Søren Larsen for sharing his *HST/WFPC2* photometry of M87 GCs. E. W. P. gratefully acknowledges the support of the Peking University Hundred Talent Fund (985). A. J. acknowledges support from the Chilean Center of Excellence in Astrophysics and Associated Technologies, and from the Chilean Center for Astrophysics FONDAF 15010003. This research has made use of the NASA/IPAC Extragalactic Database (NED) which is operated by the Jet Propulsion Laboratory, California Institute of Technology, under contract with the National Aeronautics and Space Administration.

Facilities: HST(ACS,WFPC2)

APPENDIX

THE GC LUMINOSITY FUNCTIONS OF M87 GC POPULATIONS

The quality and completeness of our photometry also allows us to fit the luminosity function of the M87 GCs. The color-magnitude diagram in Figure 4 hints that the luminosity functions of the blue and red GC subpopulations have different means and widths. We quantify this by fitting the *I*-band luminosity functions of the GC subpopulations with two different functions: a Gaussian and an evolved Schechter function (see Jordán et al. 2007). We fit only GCs with $I < 24$ mag, a limit above which neither contamination nor completeness is a problem, but which is still $\gtrsim 1\sigma$ fainter than the mean in a Gaussian parametrization. We divide blue from red GCs at $(V - I) = 1.04$, the color at which a GC is equally likely to belong either to the blue or red subpopulation according to a double Gaussian homoscedastic fit using the Kaye’s Mixture Model (KMM; McLachlan & Basford 1988; Ashman, Bird, & Zepf 1994). The results of our fits are presented in Table 3, and the luminosity distributions with fits are shown in Figure 8. We note that although we have plotted the GC magnitude distributions in bins, the fits were performed on the unbinned data using maximum likelihood estimation. There appears to be an excess of faint objects at $I > 24$ mag which are likely to be compact background galaxies.

The best-fit Gaussian parameters of the total population are $\mu_I = 22.53 \pm 0.05$ and $\sigma = 1.37 \pm 0.04$. This is nearly identical to the measurement by Kundu et al. (1999) of $\mu_{I,K99} = 22.55 \pm 0.06$ and $\sigma_{I,K99} = 1.41 \pm 0.11$. Using a distance to M87 of 16.5 Mpc ($m - M = 31.09$), our measurement translates to $\mu_{M_I} = -8.56 \pm 0.05$ mag.

The Gaussian mean of the blue GC subpopulation is expected to be brighter than that of the red GC subpopulation if the GC mass function is universal across metallicity (e.g., Ashman, Conti, & Zepf 1995; Puzia et al. 1999; Jordán et al. 2002; Jordán et al. 2007). When fitting the individual subpopulations, we find that $\mu_{I,blue} = 22.24 \pm 0.06$ mag and $\mu_{I,red} = 22.77 \pm 0.09$ mag (or $\mu_{M_I} = -8.85$ mag and -8.32 mag, respectively). This difference, $\mu_{I,blue} - \mu_{I,red} = -0.43$ mag, is consistent with what Puzia et al. (1999) find for the GC system of M49.

The Gaussian widths of the GCLFs for the two subpopulations are also different. We measure $\sigma_{I,blue} = 1.25 \pm 0.05$ mag and $\sigma_{I,red} = 1.45 \pm 0.06$ mag. The LF of the blue GCs is narrower than that for the red GCs, but is not as narrow as the mean widths for GCLFs of early-type dwarf galaxies in the Virgo and Fornax clusters, which can have $\sigma \sim 1.0$ mag (Jordán et al. 2006, 2007; Miller & Lotz 2007).

We also fit an evolved Schechter function, as defined by Jordán et al. (2007), equation 8. We fix the faint end slope of the cluster initial mass function to have a power law exponent $\beta = 2$, as was done in Jordán et al. (2007). The evolved Schechter function then has two free parameters, which we represent as m_c , the absolute magnitude of the exponential “cutoff” associated with the bright end of the Schechter function, and δ , the absolute magnitude representing the average mass loss per cluster over a Hubble time (for details, see Jordán et al. 2007, Section 3.2). The fitted parameters for all GCs (with $I < 24$ mag) are $m_{c,I} = -11.72 \pm 0.23$ mag and $\delta_I = -8.63 \pm 0.08$ mag. For the blue and red subpopulations, we find that $m_{c,I,blue} = -11.06 \pm 0.36$ mag, $m_{c,I,red} = -12.14 \pm 0.32$, $\delta_{I,blue} = -9.27 \pm 0.15$, and $\delta_{I,red} = -8.28 \pm 0.10$.

REFERENCES

- Anderson, J., & King, I. R. 2006, Instrument Science Report ACS 2006-01, 34 pages, 1
- Ashman, K. M., Bird, C. M., & Zepf, S. E. 1994, *AJ*, 108, 2348
- Ashman, K. M., Conti, A., & Zepf, S. E. 1995, *AJ*, 110, 1164
- Bailin, J., & Harris, W. E. 2009, arXiv:0901.2302
- Bertin, E., & Arnouts, S. 1996, *A&AS*, 117, 393
- Blakeslee, J. P., Anderson, K. R., Meurer, G. R., Benítez, N., & Magee, D. 2003, *Astronomical Data Analysis Software and Systems XII*, 295, 257
- Blakeslee, J. P., et al. 2009, *ApJ*, 694, 556

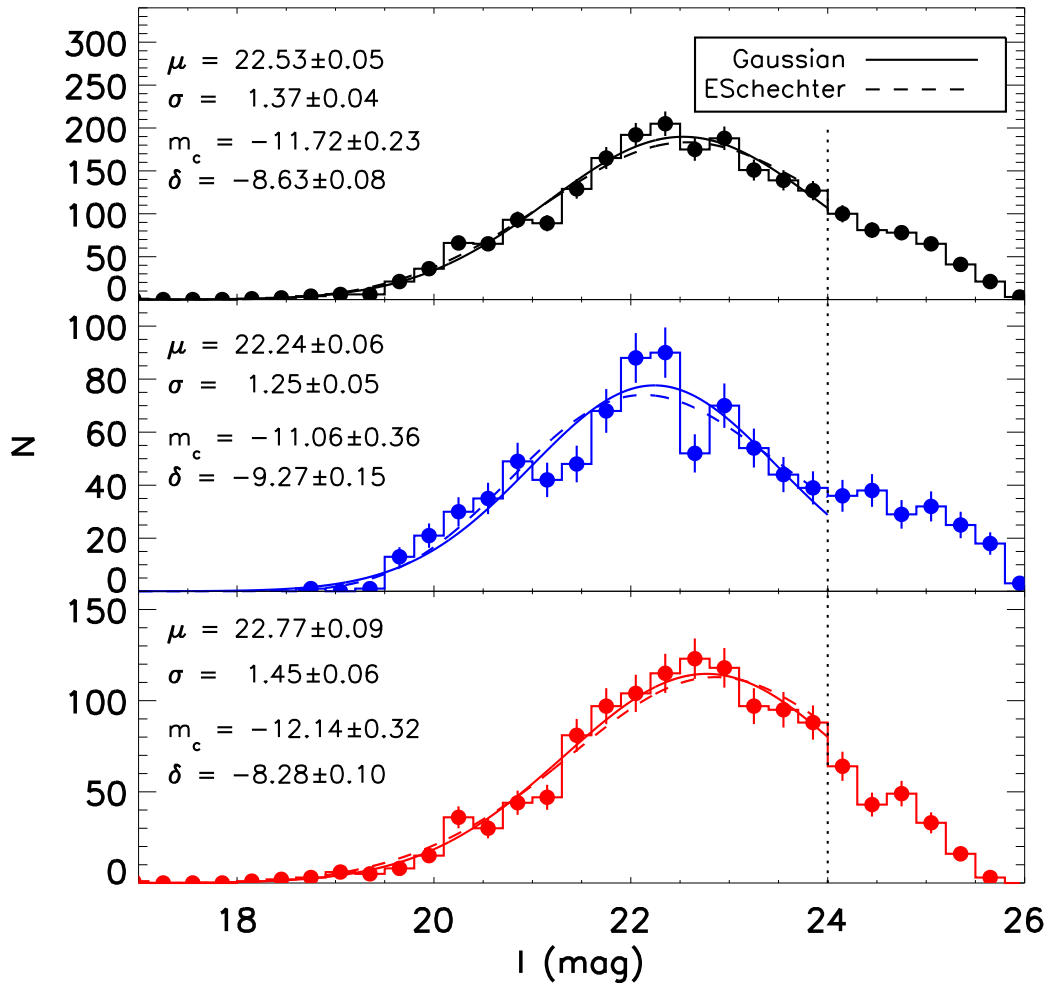


FIG. 8.— The luminosity functions of M87 GCs, divided by color. We plot the luminosity functions of all observed GCs (top), blue GCs with $(V - I) < 1.04$ (middle) and red GCs with $(V - I) > 1.04$. We performed parametric fits to the GCs with $I < 24$ (marked by dotted line) using both Gaussian (solid curve) and evolved Schechter (dashed curve) functional forms. The best-fit parameters for each function are listed in the plots and in Table 3. The blue GCs have a brighter peak and a narrower width than do the red GCs.

Brodie, J. P., & Huchra, J. P. 1991, *ApJ*, 379, 157
Cantiello, M., Blakeslee, J. P., & Raimondo, G. 2007, *ApJ*, 668, 209
Cantiello, M., & Blakeslee, J. P. 2007, *ApJ*, 669, 982
Côté, P., et al. 2004, *ApJS*, 153, 223
D’Ercole, A., Vesperini, E., D’Antona, F., McMillan, S. L. W., & Recchi, S. 2008, *MNRAS*, 391, 825
DeGraaff, R. B., Blakeslee, J. P., Meurer, G. R., & Putman, M. E. 2007, *ApJ*, 671, 1624
Forte, J. C., Faifer, F., & Geisler, D. 2007, *MNRAS*, 382, 1947
Freedman, W. L., et al. 2001, *ApJ*, 553, 47
Fruchter, A. S., & Hook, R. N. 2002, *PASP*, 114, 144
Harris, W. E., Whitmore, B. C., Karakla, D., Okoń, W., Baum, W. A., Hanes, D. A., & Kavelaars, J. J. 2006, *ApJ*, 636, 90
Harris, W. E., 2009, *ApJ*, submitted
Harris, W. E., Kavelaars, J. J., Hanes, D. A., Pritchett, C. J., & Baum, W. A. 2009, *AJ*, 137, 3314
Haşegan, M., et al. 2005, *ApJ*, 627, 203
Jordán, A., Côté, P., West, M. J., & Marzke, R. O. 2002, *ApJ*, 576, L113
Jordán, A., et al. 2004, *ApJS*, 154, 509
Jordán, A., et al. 2005, *ApJ*, 634, 1002
Jordán, A., et al. 2006, *ApJ*, 651, L25
Jordán, A., et al. 2007, *ApJS*, 171, 101 (Paper XII)
Jordán, A., et al. 2009, *ApJS*, 180, 54
King, I. R. 1966, *AJ*, 71, 64

Kundu, A., Whitmore, B. C., Sparks, W. B., Macchetto, F. D., Zepf, S. E., & Ashman, K. M. 1999, *ApJ*, 513, 733
Kundu, A. 2008, *AJ*, 136, 1013
Larsen, S. S., Brodie, J. P., Huchra, J. P., Forbes, D. A., & Grillmair, C. J. 2001, *AJ*, 121, 2974
Lee, M. G., Park, H. S., Kim, E., Hwang, H. S., Kim, S. C., & Geisler, D. 2008, *ApJ*, 682, 135
McLachlan, G. J., & Basford, K. E. 1988, *Mixture Models: Inference and Application to Clustering* (New York: M. Dekker)
McLaughlin, D. E. 1999, *AJ*, 117, 2398
Mei, S., et al. 2005a, *ApJS*, 156, 113
Mei, S., et al. 2005, *ApJ*, 625, 121
Mieske, S., et al. 2006, *ApJ*, 653, 193
Mieske, S., et al. 2008, *A&A*, 487, 921
Miller, B. W., & Lotz, J. M. 2007, *ApJ*, 670, 1074
Peng, E. W., et al. 2006a, *ApJ*, 639, 95
Peng, E. W., et al. 2006b, *ApJ*, 639, 838
Peng, E. W., et al. 2008, *ApJ*, 681, 197
Piotto, G., et al. 2007, *ApJ*, 661, L53
Puzia, T. H., Kissler-Patig, M., Brodie, J. P., & Huchra, J. P. 1999, *AJ*, 118, 2734
Schlegel, D. J., Finkbeiner, D. P., & Davis, M. 1998, *ApJ*, 500, 525

- Sirianni, M., Jee, M.J., Bentez, N., Blakeslee, J.P., Martel, A.R., Meurer, G., Clampin, M., De Marchi, G., Ford, H.C., Gilliland, R., Hartig, G.F., Illingworth, G.D., Mack, J., & McCann, W.J. 2005, *PASP*, 117, 1049
- Spitler, L. R., Larsen, S. S., Strader, J., Brodie, J. P., Forbes, D. A., & Beasley, M. A. 2006, *AJ*, 132, 1593
- Strader, J., Brodie, J. P., Spitler, L., & Beasley, M. A. 2006, *AJ*, 132, 2333 (S06)
- Strader, J., & Smith, G. H. 2008, *AJ*, 136, 1828
- Tamura, N., Sharples, R. M., Arimoto, N., Onodera, M., Ohta, K., & Yamada, Y. 2006, *MNRAS*, 373, 601
- Tonry, J. L., Blakeslee, J. P., Ajhar, E. A., & Dressler, A. 1997, *ApJ*, 475, 399
- Tonry, J. L., Dressler, A., Blakeslee, J. P., Ajhar, E. A., Fletcher, A. B., Luppino, G. A., Metzger, M. R., & Moore, C. B. 2001, *ApJ*, 546, 681
- Waters, C. Z., Zepf, S. E., Lauer, T. R., Baltz, E. A., & Silk, J. 2006, *ApJ*, 650, 885
- Waters, C. Z., Zepf, S. E., Lauer, T. R., & Baltz, E. A. 2009, *ApJ*, 693, 463
- Wehner, E. M. H., Harris, W. E., Whitmore, B. C., Rothberg, B., & Woodley, K. A. 2008, *ApJ*, 681, 1233
- Yoon, S.-J., Yi, S. K., & Lee, Y.-W. 2006, *Science*, 311, 1129

TABLE 3
BEST-FIT PARAMETERS FOR *I*-BAND GC LUMINOSITY FUNCTIONS

Sample	Gaussian			Evolved Schechter	
	μ_I	μ_{M_I}	$\sigma_{I,\text{all}}$	$m_{c,I}$	δ_I
All	22.53 ± 0.05	-8.56 ± 0.05	1.37 ± 0.04	-11.72 ± 0.23	-8.63 ± 0.08
Blue	22.24 ± 0.06	-8.85 ± 0.06	1.25 ± 0.05	-11.06 ± 0.36	-9.27 ± 0.15
Red	22.77 ± 0.09	-8.32 ± 0.09	1.45 ± 0.06	-12.14 ± 0.32	-8.28 ± 0.10

Notes: All parameters have units of magnitudes. Blue and red GCs are divided at $(V - I) = 1.04$ mag. Fits are performed on GCs with $I < 24$ mag. Absolute magnitudes assume $m - M = 31.09$.